Stabilization of telomere G-quadruplexes interferes with human herpesvirus 6A chromosomal integration.

Shella Gilbert-Girard[1], Annie Gravel[1], Sara Artusi[2], Sara N. Richter[2], Nina Wallaschek[3], Benedikt B. Kaufer[3] and Louis Flamand[1,4]

Running title: HHV-6A integration and telomeric G4 stabilization

[1]Division of Infectious Disease and Immunity, CHU de Québec Research Center, Quebec City, Quebec G1V 4G2, Canada; [2]Department of Molecular Medicine, University of Padua, via Gabelli, 63, 35121 Padua, Italy; [3]Institut für Virologie, Freie Universität Berlin, Berlin 14163, Germany and [4]Department of microbiology, infectious disease and immunology, Faculty of Medicine, Université Laval, Quebec City, Québec, G1V 0A6 Canada

***To whom correspondence should be addressed:**
Louis Flamand PhD MBA
Division of Infectious Disease and Immunity
Room T1-49
CHU de Quebec Research Center,
Quebec city, Canada
G1V 4G2

Tel (418)-525-4444 ext 46164; Fax (418)-654-2765
Email:Louis.flamand@crchul.ulaval.ca

Word count abstract: 223

Word count text:5121

Abstract

Human herpesvirus 6A and 6B (HHV-6A/B) can integrate their genomes into the telomeres of human chromosomes using a mechanism that remains poorly understood. To achieve a better understanding of the HHV-6 integration mechanism, we made use of BRACO-19, a compound that stabilizes G-quadruplex secondary structures and prevent telomere elongation by the telomerase complex. First, we analyzed the folding of telomeric sequences into G-quadruplex structures and their binding to BRACO-19 using G-quadruplex specific antibodies and surface plasmon resonance. Circular dichroism studies indicate that BRACO-19 modifies the conformation and greatly stabilizes the G-quadruplexes formed in G-rich telomeric DNA. Subsequently we assessed the effects of BRACO-19 on HHV-6A initial phase of infection. Our results indicate that BRACO-19 does not affect entry of HHV-6A DNA into cells. Next, we investigated if stabilization of G-quadruplexes by BRACO-19 affected HHV-6A ability to integrate its genome into host chromosomes. Incubation of telomerase expressing cells with BRACO-19, such as HeLa and MCF-7, caused a significant reduction in the HHV-6A integration frequency ($p<0.002$); in contrast, BRACO-19 had no effect on HHV-6 integration frequency in U2OS cells that lack telomerase activity and elongate their telomeres through alternative lengthening mechanisms. Our data suggest that the fluidity of telomeres is important for efficient chromosomal integration of HHV-6A and that interference with telomerase activity negatively affect the generation of cellular clones containing integrated HHV-6A.

Importance

Human herpesvirus 6A/B (HHV-6A/B) can integrate their genomes into the telomeres of infected cells. Telomeres consist of repeated hexanucleotides (TTAGGG) of varying length (up to several kilobases) and end with a single-stranded 3' extension. To avoid recognition and induce a DNA-damage response, the single-stranded overhang folds back on itself and forms a telomeric loop (T-loop) or

adopts a tertiary structure referred to as G-quadruplex. In the current study, we have examined the effects of a G-quadruplex binding and stabilizing agent, BRACO-19, on HHV-6A chromosomal integration. By stabilizing G-quadruplex structures, BRACO-19 affects the ability of the telomerase complex to elongate telomeres. Our results indicate that BRACO-19 reduces the number of clones harboring integrated HHV-6. This study is the first of its kind and suggests that telomerase activity is likely essential to restore a functional telomere of adequate length following HHV-6A integration.

Introduction

Human herpesvirus 6A (HHV-6A) and HHV-6B are two distinct DNA viruses that belong to the subfamily *Betaherpesvirinae*. Despite their high genome sequence similarities, these viruses possess different biological and epidemiological properties (1). HHV-6B is a ubiquitous virus that infects almost 100% of the human population. It is the etiological agent of the febrile illness *roseola infantum*, also known as the sixth childhood eruptive disease (2, 3). Reactivation of HHV-6B in immunosuppressed individuals is associated with adverse clinical outcomes including life-threatening encephalitis or graft rejection in transplant patients (4). The diseases associated with HHV-6A infection are not clearly established. During latency, human herpesviruses typically maintain their genomes as extrachromosomal nuclear episomes. How HHV-6A/B achieve latency is still unclear and since these viruses can integrate their genomes into host chromosomes integration is considered one possible mode of latency (5). HHV-6 integration was first described by Luppi et al., who observed the presence of the integrated HHV-6 genome in the chromosomes of freshly isolated peripheral blood mononuclear cells (PBMC) (6, 7). HHV-6A/B integration can occur in germinal cells and be transmitted vertically to descendants (8, 9). This condition is termed inherited chromosomally integrated HHV-6 (iciHHV-6) and is present in about 0.2% to 1% of the human population across the world (reviewed in (10, 11)). In 2015, Gravel et al. analyzed DNA samples from 20,000 Quebecers (Canada) for iciHHV-6 and concluded that iciHHV-6A/B represents a predisposing risk factor for angina pectoris (12).

HHV-6A/B integration can occur in various chromosomes, with viral genomes consistently detected in telomeric regions that are located at chromosome termini (5, 10, 13-15). Telomeres are composed of double-stranded TTAGGG repeats (8-13 kbp long) followed by a 30 to 200 bp single-stranded 3' overhang (16-19). Telomeres protect the chromosome against information loss and instability (20, 21) and are shortened every time a cell divides. The HHV-6A/B genome consists of a unique sequence (U)

that is flanked by G-rich direct repeat regions (DR) that harbor the packaging sequences (*pac*1 and *pac*2) and two arrays of either perfect or imperfect telomeric repeats (TMR) at the genome termini (22-26). The presence of these repeats at the ends of the viral genomes and the fact that chromosomal integration occurs in telomeres, led to the hypothesis that HHV-6A/B integrates the human genome by homologous recombination (HR) between viral TMRs and chromosomal telomeric sequences (27, 28). Wallaschek et al. recently demonstrated that the viral telomeric repeats are required for efficient HHV-6A integration into host telomeres (29). Analysis of the integrated virus genome revealed that the perfect TMR of the DR_R region are fused to the host chromosome accompanied by a loss of the *pac*2 sequence, consistent with an integration mediated by HR between the viral TMR and the host telomere (5). At the other end of the viral genome, the *pac*1 region is also lost and additional telomeric repeats are added, suggesting that the TMR in DR_L is a substrate for the generation of a new telomere (30-32).

It has been shown that nucleic acids G-rich sequences, such as those at telomeres, can fold into peculiar secondary structures called G-quadruplexes (33). Four Gs bind via Hoogsteen-type hydrogen bonds base-pairing to yield G-quartets: stacking of at least two G-quartets leads to formation of the G-quadruplex, through π-π interactions between aromatic systems of G-quartets. K^+ cations in the central cavity relieve repulsion among oxygen atoms and specifically support G-quadruplex formation and stability (34). Biologically relevant G-quadruplexes normally form intramolecular structures that, based on the strand orientation, can adopt three main topologies: parallel, antiparallel, and hybrid-type (35).

In this work, we set to determine whether a loss in telomere fluidity would affect the ability of HHV-6A to integrate its genome into host DNA. To achieve this, we used BRACO-19, a 3,6,9-trisubstituted acridine derivative designed by molecular modelling to interact with and stabilize the G-quadruplex

103 DNA structures formed in human telomeres, while displaying very low affinity towards duplex DNA
104 (36). BRACO-19 binds and stabilizes G-quadruplexes present in the single-stranded region of
105 telomeres. BRACO-19 also inhibits telomerase activity and provokes the displacement of the
106 telomerase complex (37, 38).
107 In the current study, we first confirmed the specificity of BRACO-19 and next assessed its effect on
108 HHV-6A integration. Our results demonstrate that BRACO-19 does not affect cell viability or HHV-6A
109 entry as determined by measuring the amount of intracellular viral DNA. BRACO-19 did however
110 affect HHV-6A ability to integrate its genome in HeLa and MCF-7 cells. Taken together, our data
111 provide the evidence that a fluid interaction between HHV-6A genome and the telomeres is needed
112 for chromosomal integration.
113

114 **Results**

115 **Biophysical characterization of BRACO-19 binding to G-quadruplex telomere structures**
116 To ensure the correct folding of oligonucleotides into G-quadruplex structures, we initially performed
117 an ELISA assay using the BG4 and 1H6 antibodies that specifically bind to G-quadruplex structures.
118 We demonstrated that the BG4 antibodies preferentially bind G-rich oligonucleotides, such as the
119 telomeric ($(TTAGGG)_4$) and the myc oligonucleotide. The latter corresponds to a DNA sequence
120 present in the promoter of the MYC gene and previously reported to fold into a G-quadruplex
121 structure (39-41) (Figure 1). Binding of 1H6 antibodies to G-rich oligonucleotides $(TTAGGG)_4$ was also
122 observed. Marginal binding to the ss-DNA was recorded, as previously reported (42, 43). These results
123 confirm that in our conditions both the telomeric and myc oligonucleotides fold into G-quadruplexes.
124

125 Next, we analyzed the binding of BRACO-19 to the telomeric and myc oligonucleotides by surface
126 plasmon resonance. BRACO-19 was designed to bind specifically to G-quadruplexes with the
127 assumption that each of its chains would occupy a groove of its ligand, as it stacks between two G-
128 quadruplexes: its aromatic planar core stacks between two G-quadruplexes and each of the two
129 positively charged chains occupy the groove of each bound G-quadruplex (36, 37, 44). As positive
130 control, the BG4 antibody was used. BG4 antibody efficiently bound the G-quadruplex-folded
131 telomeric sequence (K_D = 5.46x10^{-7} M) and the myc promoter sequence (K_D = 2.52x10^{-8} M), confirming
132 the ELISA results. Much weaker (100x less than that of myc) binding of the BG4 antibody was
133 observed against the C-rich telomeric sequence (K_D = 1.31x10^{-6}M). The binding of BRACO-19 was
134 studied next. As shown, BRACO-19 efficiently binds to both G-rich telomeric and myc G-quadruplex
135 oligonucleotides with K_Ds in the range of 10^{-8} M. In contrast, minimal binding to the C-rich telomeric
136 sequence was observed and no constant could be calculated (Figure 2-F). These results confirm that
137 BRACO-19 specifically binds to oligonucleotides forming G-quadruplex structures.
138
139 Folding of HHV-6A *pac1* and telomeric DNA into G-quadruplex and binding of BRACO-19 to the
140 telomeric DNA were confirmed by circular dichroism (CD) analysis. HHV-6A *pac1* sequence exhibited a
141 parallel G-quadruplex topology (minimum near 240 nm and maximum near 260 nm), characterized by
142 very high molar ellipticities (Figure 3A-B). Stability of the telomeric G-quadruplex was measured by
143 thermal unfolding: T_m, i.e. the melting temperature obtained at half unfolding. The *pac1* sequence
144 was very stable in the absence of K^+ with T_m of 67˚C whereas the addition of K^+ (100 mM) further
145 stabilized the G-quadruplex structure (T_m >100˚C). The telomeric G-quadruplex folded oligonucleotide
146 displays a CD spectrum characteristic of a hybrid type conformation (maximum near 290 nm and
147 shoulder near 260 nM) (Figure 3C) (35). Upon addition of BRACO-19, the CD spectrum drastically

148 changed with an increase in the two positive peaks at 290 and 240 nm, and formation of a negative
149 peak at 260 nm, signals that have been empirically shown to be signatures of the antiparallel G-
150 quadruplex topology (Figure 3D) (35). The T_m of the telomeric sequence in the absence of BRACO-19
151 was 66.8°C and it increased to values > 90°C in the presence of the compound, with a net variation in
152 T_m > 23.2°C. These results indicate HHV-6A pac1 sequence can fold into G-quadruplex and that
153 BRACO-19 specifically binds and greatly stabilizes G-quadruplex structures.
154
155 **Toxicity analyses of BRACO-19**
156 To assess BRACO-19 concentrations to be used without induction of cytotoxic effects, we performed
157 MTT cell proliferation assays in U2OS, HeLa and MCF-7 cells. The cells were incubated for three days
158 with varying concentrations of BRACO-19 ranging from 0 to 2 µM. No toxicity was observed with
159 BRACO-19 concentrations up to 1 µM (Figure 4). A concentration of 2 µM reduced the survival and
160 proliferation of all cell types. All experiments were thus performed with concentrations of BRACO-19
161 $\leq$ 1µM.
162
163 **Effects of BRACO-19 on HHV-6 DNA levels**
164 The HHV-6 genome contains G-rich sequences, including telomeric repeats that might interact with
165 BRACO-19 and affect viral genome replication. We determined the amount of HHV-6 DNA at different
166 times post infection in BRACO-19 treated or untreated cells. U2OS, HeLa and MCF-7 cells were
167 infected with HHV-6A (U1102) for 4h, 48h or 72h in the absence or in the presence of BRACO-19 (1
168 µM). Intracellular DNA was extracted and the amount of HHV-6A DNA was assessed by qPCR. We
169 could demonstrate that for most time points tested (except for the 4h in U2OS cells), BRACO-19 had
170 no impact on intracellular viral DNA levels (Figure 5A), indicating that the compound had limited

171 effects on virus entry or the fate of the HHV-6 genome. The fact that we observed a significant
172 decrease in viral DNA at 48h and 72h suggests that the cellular environment of these 3 cell lines does
173 not allow efficient HHV-6 DNA replication. As suggested (45), semi-permissive or non-permissive cells
174 are preferred cell types for the study of viral integration since permissive cells are for the most part
175 destroyed during productive infection. In support, even though immediate-early (IE1) and early (P41)
176 proteins could be detected in 10-20% of U2OS cells (figure 5B), expression of late proteins and release
177 of mature virions in the culture supernatant was not detected (data not shown).
178

179 **Effects of BRACO-19 on HHV-6 chromosomal integration**

180 We next examined the effects of the BRACO-19 on HHV-6A chromosomal integration. The frequency
181 of HHV-6A/B integration was determined using recently described two integration assays, one based
182 on the isolation of cell clones and the other using bulk cultures, that provide equivalent estimates
183 (45). Using these assays, most clones analyzed contained approximately 1 copy of HHV-6A/B
184 genome/cell, as determined by *in situ* hybridization and droplet digital PCR (ddPCR) (45). For the first
185 three experiments, HeLa and U2OS cells were either left untreated or treated with 1µM BRACO-19
186 prior to and during infection. After 48h, the medium was changed and cells were seeded in 96-well
187 plates and left without BRACO-19 for the rest of the experiment. For the fourth assay, cells were left
188 with BRACO-19 for 72h and the concentration was subsequently reduced to 0.1 µM for the rest of the
189 experiment to determine whether a longer exposition to BRACO-19 would affect the outcome of the
190 experiment. Single cell cloning was performed and the frequency of clones containing
191 chromosomally-integrated HHV-6 (ciHHV-6^{+}) was determined by qPCR from the four independent
192 experiments (Table 1). In HeLa cells, BRACO-19 treatment resulted in a 45% reduction in HHV-6A
193 integration frequency relative to the untreated control cells (P = 0.0017). In contrast, no statistically

194 significant difference (p=1.00) was observed in the HHV-6 integration frequency of U2OS cells treated
195 with BRACO-19 compared to untreated cells. Prolonging the exposition to BRACO-19 had no
196 additional effects on the proportion of ciHHV-6$^+$ clones obtained. To ensure that clones contained
197 integrated HHV-6A, we performed FISH analyses on several clones. A representative result is
198 presented in figure 5C.

199

200 To confirm these results, we included an additional cell line, MCF-7, and used the ddPCR analysis
201 platform that allowed the detection of ciHHV-6$^+$ cells in polyclonal population without the need to
202 produce individual clones. BRACO-19 treated and untreated HeLa, MCF-7 and U2OS cells were
203 infected with HHV-6A and allowed to grow for approximately 1 month. Cellular DNA was isolated and
204 the percentage of cells containing integrated HHV-6A was determined by ddPCR, as described (45).
205 ddPCR analyses confirmed that the integration frequency was significantly reduced in HeLa (52.66%)
206 (p=0.010) and MCF-7 cells (51.05%) (p=0.009) treated with BRACO-19 (Table 2). A reduction of 20% of
207 the integration frequency was observed in U2OS cells in presence of BRACO-19, but it did not reach
208 statistical significance (p=0.056). Taken together, our data suggests that integration of the viral
209 genome is significantly reduced in HeLa and MCF-7 cells treated with BRACO-19, but not in
210 telomerase negative U2OS.

211

212 **Discussion**

213 Although HHV-6A/B chromosomal integration was first thought to be an evolutionary dead-end, it is
214 now thought to be a way HHV-6A/B and several other herpesviruses that harbor telomeres at their
215 genome ends maintain their virus genome during latency (46). The integrated virus genome can be

excised from latently infected cells and re-initiate lytic replication (5, 47-50). Certain HHV-6A/B proteins, such as U94, possess many characteristics, such as exonuclease and helicase activities, a preferential DNA binding to telomeric sequences and the ability to hydrolyze ATP that are compatible with a role in viral integration (51). However, recent results indicate that U94 is dispensable for HHV-6A integration *in vitro* (52). HHV-6A/B chromosomal integration is thought to occur via homologous recombination. Viral integration always occurs in telomeres and it has been shown that the viral telomeric sequences are essentials for efficient integration (29). Even though the formal integration mechanism has yet to be demonstrated experimentally, sequencing of ciHHV-6A/B indicates that the TMR of the DR_R of the genome is fused to the host chromosome telomeric repeats with loss of *pac*2 sequence from DR_R. Such a structure is compatible with HR-mediated viral integration (5, 31, 32).

To better understand the HHV-6A integration process, we made use of BRACO-19, a compound that stabilizes G-quadruplex structures (37, 38). The binding of BRACO-19 to telomeric G-quadruplexes was confirmed by surface plasmon resonance while circular dichroism spectra coupled with melting analyses indicated that BRACO-19 stabilizes the G-quadruplex structure. Considering that HR is a dynamic process that requires that two sequences bind together and elongate with the intervention of a polymerase, we expected that the rigidity of the telomeres, and possibly the viral TMRs as well, in the presence of BRACO-19 would affect chromosomal integration. Indeed, we observed that in HeLa and MCF-7 cells, the frequency of chromosomal integration was reduced by about 50% when exposed to the drug. The reduction in integration frequency is not due to negative effects of BRACO-19 on HHV-6A entry, as no difference in viral genome copy numbers was observed between mock and BRACO-19-treated cells (Figure 4). Furthermore, considering that HR operates before cells enter mitosis, during and shortly after the S and G2 of the cell cycle (53), we have confirmed that BRACO-19

239 did not influence cell cycle progression under the tested experimental conditions tested (data not
240 shown). Thus, reduced fluidity of telomeric sequences negatively affected the ability to generate
241 clones of cells with integrated virus. In contrast to HeLa and MCF-7 cells, no statistically significant
242 effects of BRACO-19 on the frequency of HHV-6A chromosomal integration in U2OS cells were noted.
243 Several hypotheses may be formulated to explain this difference: first, HeLa and MCF-7 cells express
244 telomerase and use this enzyme to elongate their telomeres. Upon viral integration, the viral TMR on
245 the left end (from the DR_L) of the genome is short and must be elongated to prevent cells from
246 entering senescence. Inhibition of telomerase activity by stabilization of the G-quadruplex viral
247 telomere likely prevents telomere elongation early after integration and may cause cells containing
248 the integrated HHV-6A genome to die prematurely. In contrast, U2OS cells do not express telomerase
249 and use an alternative telomere elongation mechanism (ALT). ALT is mostly based on HR (54) and
250 repression of HR appears to be loosened in ALT+ cells to allow telomere maintenance, which might be
251 the cause of the more frequent homologous recombination and telomere sister chromatid exchange
252 observed in these cells (55, 56). In ALT+ cells, the viral telomere likely gets elongated by HR, in a
253 manner similar to host cell telomeres. Second, it was recently reported that ALT+ cells have much
254 longer telomeric overhang (40-400 nucleotides) (57) relative to telomerase positive cells (65-140
255 nucleotides) (58). This difference in telomeric overhang length may influence the folding of the
256 telomeric DNA into G-quaduplex and affect BRACO-19 binding. Thirdly, another important difference
257 between ALT+ and telomerase expressing cells is the frequent association of the promyelocytic
258 leukemia protein (PML) nuclear bodies at telomeres in ALT+ cells (59, 60). In addition to PML, these
259 ALT-associated PML nuclear bodies (APBs) contain many other proteins that form ring-like structures
260 around the telomeric DNA that may negatively influence DNA folding or affect BRACO-19 binding.
261 Furthermore, some of these proteins present at telomeres of ALT+ cells include the BLM and WRN

RecQ helicases that bind telomeric DNA (61-63) and can unwind G-quadruplex structures (64-66) thereby limiting the potential number of G-quadruplex structures. Considering that ligands that stabilize G-structures are also reported to inhibit the processivity of these enzymes (67), the net *in vivo* impact of G-quadruplex unfolding by helicases and stabilization by BRACO-19 remains to be determined.

The presence of G-quadruplex in viral genomes was previously reported (reviewed in (68)). Interestingly, BRACO-19 negatively affects the genome processing activities such as replication and transcription of HSV-1 (69), EBV (70), and HIV-1 (71). Unlike these viruses however, *in* silico analyses of the HHV-6A/B genomes indicate that potential G-quadruplex structures are located exclusively in the viral TMR and not within coding regions (71). BRACO-19 is therefore not expected to affect the expression of HHV-6A/B genes. Whether BRACO-19 affects viral DNA replication is yet to be studied in detail. The cell lines used in this study are not very permissive to HHV-6A infection/replication and thus are not adequate to address the effects of BRACO-19 on viral DNA replication. However, considering that HHV-6A TMRs, located at the extremities of the viral genome, that contain telomeric and *pac1* sequences that can fold into G-quadruplex (Figure 3) and likely to form similar structures during viral DNA unwinding and replication, one might expect BRACO-19 to affect viral replication or DNA packaging. Analysis of the HHV-6B *pac1* sequence also indicates folding into a parallel G-quadruplex structure (data not shown). Thermal unfolding studies indicate that relative to HHV-6A *pac1* (63% GC), HHV-6B *pac1* (59% GC) was less stable with T_m of 57˚C and a T_m of 67˚C in the absence or in the presence of 100 mM KCl, respectively. How and if this variation in G-quadruplex stability of *pac1* sequences translates into biological differences during HHV-6A and HHV-6B infection or integration remains to be determined.

284 In summary, we presented data indicating that the G-quadruplex stabilizing agent BRACO-19
285 negatively affects HHV-6A integration in telomerase expressing cells. Our results suggest that
286 following the recombination between the host and viral telomeres at one end of the virus genome,
287 the viral telomere at the other DR_L end needs to be rapidly elongated. If this event is prevented,
288 through the action of BRACO-19 that inhibits telomerase activity, expansion of clones with integrated
289 virus is compromised. It is well established that the self-renewal potential of cells is directly
290 proportional to telomere lengths and telomerase activity (72, 73). It is also known that the shortest
291 telomere, not average telomere length, is critical for cell viability and chromosome stability (74).
292 When the number of telomeric repeats falls below 13, chromosomal instability is observed (75). At
293 the time of integration, the TMR in DR_L contains approximately 50-60 repeats (23, 76). Considering
294 that with each cell division 10-20 telomeric repeats are lost (77), in the absence of elongation,
295 chromosomal instability would occur within 2-3 cell divisions. The study of DNA damage responses at
296 the extremity of the viral genome should help understand the importance of telomere elongation
297 processes following integration and its importance in preventing premature cellular senescence.
298 Lastly, based on these results we also surmise that the long-term maintenance of integrated HHV-
299 6A/B following infection of primary somatic cells that lack telomerase expression and do not have
300 telomere elongation mechanisms is improbable. To be successful, HHV-6A/B integration likely needs
301 to occur in primary cells expressing telomerase such as gametes, stem cells or activated T
302 lymphocytes, the latter being a primary HHV-6 target cells (78). In fact, T and B lymphocytes are
303 unique among differentiated somatic cell types in terms of their ability to respond to specific or
304 nonspecific stimuli by proliferation and continued expansion, accompanied by TERT upregulation (79,
305 80). However, the factors/conditions favoring integration over productive infection in highly
306 permissive cells such as T lymphocytes remain to be elucidated.

Materials and Methods

Cell lines and viruses

U2OS (osteosarcoma) cells (ATCC, Manassas, VA, USA) were cultured in Dulbecco's modified Eagle's medium (DMEM, Corning Cellgro, Manassas, VA, USA) supplemented with 10% Nu serum (Corning Cellgro), non-essential amino acids (Corning Cellgro), HEPES, sodium pyruvate (Wisent Inc., St-Bruno, Québec, Canada) and plasmocin 5 µg/ml (InvitroGen, San Diego, CA, USA). HeLa (cervix epithelial) and MCF-7 (mammary epithelial) cells (ATCC) were cultured in the same medium, but supplemented with 10% fetal bovine serum (FBS) (Thermo Fisher Scientific, Waltham, MA, USA) instead of Nu serum. HSB-2 (ATCC, CCL-120.1), human T lymphoblastic cells, were cultured in RPMI-1640 (Corning Cellgro) supplemented with 10% Nu serum (Corning Cellgro), HEPES and plasmocin 5 µg/ml (InvivoGen, San Diego, CA, USA). HHV-6A was propagated in HSB-2 as previously described (81).

BRACO-19 cytotoxicity

BRACO-19 (N,N'-(9-((4-(dimethylamino)phenyl)amino) acridine-3,6-diyl)bis(3-(pyrrolidin-1-yl) propanamide) was purchased from Sigma-Aldrich Canada. To evaluate the cytotoxic effect of BRACO-19, a 3-(4-5-dimethylthiazol-2-yl)-2,5-diphenyltetrazolium bromide (MTT) assay was performed. U2OS, HeLa and MCF-7 cells were plated at 5000 cells/well in 96-well plates (6 wells/condition). Cells were treated with increasing concentrations of BRACO-19 (0-2 µM) and incubated at 37°C. After 72h, cell survival was evaluated by adding 10 µl/well of MTT solution (TACS MTT cell proliferation assay, R&D systems). Cells were incubated 4h at 37°C and 110 µl/well of SDS-HCl solution (sodium dodecyl sulphate 10%, HCl 0.01 M) were subsequently added. Cells were incubated overnight at 37°C and the absorbance was determined at 620 nm (Infinite M200 Microplate Reader, Tecan).

Effect of BRACO-19 on HHV-6 DNA levels

To investigate the effect of BRACO-19 on the initial phase of HHV-6 infection, U2OS, HeLa and MCF-7 cells were seeded in 12-well culture plates at $8x10^4$ (U2OS) or $4x10^4$ (HeLa, MCF-7) cells/well and treated before (2h) and during HHV-6A infection (MOI of 1) for 4h at 37°C. Cells were then washed three times with PBS and cultured in complete medium with or without BRACO-19 (1µM). After 4h, two and three days of infection, cells were washed extensively, treated with trypsin to remove attached virions and detached cells and washed again before DNA isolation using QIAamp DNA blood mini kit (Qiagen Inc., Toronto, ON, Canada) following the manufacturer's instructions. 100 ng of DNA were analyzed by qPCR with a Rotor-Gene Q (Qiagen) using the Rotor-Gene Multiplex PCR Kit (Qiagen) and HHV-6-specific primers as previously described (82). As a cellular control, GAPDH-specific probe and primers (IDT) were used with the following sequences: FWD 5'-GTCCCTCAATATGGTCCTGTC-3', REV 5'- TTCTCCATGGTGGTGAAGAC-3' and probe 5'-/5HEX/CGACGTACT/ZEN/CAGCGCCAGCATC/3IABkFQ/-3'.

G-quadruplex specific antibodies.

The pSANG10-3F-BG4 plasmid was a gift from the laboratories of S. Balasubramanian and J. McCafferty (Addgene plasmid # 55756) (42). The single chain Flag-BG4 antibody was expressed in *E. coli* and purified by affinity chromatography, as described (42). The 1H6 monoclonal antibody (43) was a gift from P. Lansdorp.

ELISA

The ELISA was performed with the BG4 or 1H6 antibodies that bind specifically to the G-quadruplex structures (42, 43). Biotinylated-oligonucleotides of the Myc promoter (5'-Biosg/ACTACTACTGGGGAGGGTGGGGAGGGTGGGGAAGG-3') and telomeric repeats (5'-Biosg/ACTACTACTGGTTAGGGTTAGGGTTAGGGTTAGGGTTAG-3') that fold in G-quadruplex and ssDNA

(5'-Biosg/ACTACTACTGGCATAGTGCGTGGGCG-3') that does support formation of G-quadruplex were purchased from IDT (Coralville, Iowa, USA). 96-well plates were coated with an avidin solution at 5 µg/ml in water at 37˚C overnight. The oligonucleotides were folded by incubation at 95˚C for 10 min in buffer (10 mM Tris-HCl pH 7.5, 100 mM KCl) and were left to cool down at RT overnight. The oligonucleotides were added to the wells at a concentration of 2 pmoles/well. The G- quadruplex specific antibody was added at different concentrations (BG4 from 0-32 nM and 1H6 from 0-266 nM). After 3 washes with PBS-Tween 0.1% (PBS-T), 1 µg/mL of anti-FLAG antibody (Applied Biological Materials, Richmond, BC, Canada) were added (for BG4 only) and the plate was incubated for 1 h at room temperature. After 3 additional washes, 0.1 mL of horseradish-peroxidase-conjugated goat anti-mouse antibody (1:20000 dilution) (Jackson ImmunoResearch Laboratories Inc., West Grove, PA, USA) were added to each well for 1 h at room temperature. After washing, the tetramethylbenzidine substrate (BD Biosciences, Mississauga, ON, Canada) was added and the reaction allowed to proceed for 15 minutes after which 0.05 mL of sulfuric acid were added. The absorbance of each well was measured at 450 nm with the Infinite M200 microplate reader.

Surface Plasmon Resonance

All SPR experiments were conducted using the ProteOn XPR36 apparatus (Bio-Rad, Mississauga, Canada). Biotin-labeled DNA oligonucleotides were attached to the surface of a neutravidin-coated NLC chip (Bio-Rad). The NLC chip was preconditioned by injecting two times sequentially, 50 mM NaOH and 1 M NaCl in the two directions (horizontally and vertically). The same biotinylated-oligonucleotides used for the ELISA (Myc, human Telo G-rich and human Telo C-rich (5'-Biosg/ACTACTACTTAACCCTAACCCTAACCCTAACCCTAACCCT-3')) were diluted to 25 nM in running buffer (10 mM Hepes-KOH pH 7.4, 0.2 M KCl, 3 mM EDTA and 0.005% Tween-20). The equivalent of 60 Response Unit (RU) of biotinylated-oligonucleotides was attached to the NLC chip. The chip was

then ready for protein binding analyses. Between each of these injections, a three-step regeneration (2 M NaCl, 5 mM NaOH + 0.5 M NaCl, 0.1% SDS) program was performed to remove residual binding. BG4 was injected at 50 μl/min over 3 min, followed by a dissociation time of 10 min. BRACO-19 was injected at 25 μl/min over 15 min, followed by a dissociation time of 30 min.

Spectroscopic analysis

HHV-6A *pac1* sequence (5'-CCCCCGGGGGGGCTAAAAAAAGGGGGGTAA -3') from U1102 strain (26) and the telomeric DNA oligonucleotide (5'-AGGGTTAGGGTTAGGGTTAGGG-3') were diluted from stock to a final concentration of 4 μM in lithium cacodylate buffer (10 mM, pH 7.4, +/- KCl 100 mM). All samples were annealed by heating at 95 °C for 5 min, gradually cooled to room temperature and measured after 24 h. BRACO-19 was added after DNA annealing at a final concentration of 16 μM. CD spectra were recorded on a Chirascan-Plus (Applied Photophysics, Leatherhead, UK) equipped with a Peltier temperature controller using a quartz cell of 5-mm optical path length and scanning a speed of 50 nm/min with a response time of 4 sec over a wavelength range of 230-320 nm. The reported spectrum of each sample represents the average of 2 scans at 20 °C and it is baseline corrected for signal contributions due to the buffer. Observed ellipticities were converted to mean residue ellipticity (θ) = deg×cm^2×dmol^{-1} (mol. ellip.). For the determination of T_m, spectra were recorded over a temperature range of 20-90 °C, with temperature increase of 5 °C/min. T_m values were calculated by the van't Hoff equation, applied for a two-state transition from a folded to unfolded state, assuming that the heat capacity of the folded and unfolded states are equal.

HHV-6 integration assay

HeLa and U2OS cells were seeded in 48-wells plates at 1x10^4 cells per well and cultured overnight. BRACO-19 (1 μM) was added to half of the wells 3 h before infection. All cells were infected at a MOI

of 5 for 4 h, washed with PBS and cultured in media with or without BRACO-19 (1 µM) for 48 h for the first three assays. Cells were then detached with trypsin, counted and seeded at 2 cells per well in 96-well plates. Wells containing more than one clone were excluded. Clones were harvested at confluence (approximately 30 days) and then detached with trypsin and grown in 24-well plates. When confluent, DNA was isolated from cells and tested for the presence of HHV-6 DNA by qPCR. In a fourth assay, cells were infected and cultured for 72h with BRACO-19 (1 µM) and then seeded in 96-well plates with or without BRACO-19 (100 nM). Medium and BRACO-19 were changed every three days for the rest of the experiment.

To confirm the above results, we measured the frequency of integrated HHV-6 in bulk cultures using droplet digital PCR (ddPCR), instead of isolating individual clones (45). Briefly, HeLa, MCF-7 and U2OS were infected using the same conditions as described above. Three days after infection, cells were transferred into a 25 cm^2 flask and cultured with or without BRACO-19 (100 nM) for 21 days. At that point in time, cells were detached using trypsin and DNA was isolated and tested by ddPCR for the presence HHV-6 and the cellular reference gene RPP30, as described previously (83). U65-U66 specific primers were validated previously (12, 84) and used for the detection of the integrated HHV-6 genome.

Statistical analyses

Clone integration frequencies were analyzed using Fisher's exact test and BRACO-19 cytotoxicity and DNA levels were analyzed using t-test. A p value < 0.05 was considered statistically significant.

ACKNOWLEDGMENTS.

416 The following study was supported by a grant from the Canadian Institutes of Health research
417 awarded to LF (MOP_123214). SGG is supported by a studentship from the Fonds de Recherche
418 Québec-Santé.

419

420 **AUTHOR CONTRIBUTIONS**

421 S.G.G., A.G., S.A., and N.W., performed experiments. L.F., B.B.K., S.N.R made contributions to the
422 design and interpretation of experiments in addition of providing key reagents. S.G.G., and L.F., wrote
423 the paper.

REFERENCES

1. **Ablashi D, Agut H, Alvarez-Lafuente R, Clark DA, Dewhurst S, DiLuca D, Flamand L, Frenkel N, Gallo R, Gompels UA, Hollsberg P, Jacobson S, Luppi M, Lusso P, Malnati M, Medveczky P, Mori Y, Pellett PE, Pritchett JC, Yamanishi K, Yoshikawa T.** 2014. Classification of HHV-6A and HHV-6B as distinct viruses. Arch Virol **159:**863-870.
2. **Yamanishi K, Okuno T, Shiraki K, Takahashi M, Kondo T, Asano Y, Kurata T.** 1988. Identification of human herpesvirus-6 as a causal agent for exanthem subitum. Lancet **1:**1065-1067.
3. **Tesini BL, Epstein LG, Caserta MT.** 2014. Clinical impact of primary infection with roseoloviruses. Curr Opin Virol **9:**91-96.
4. **Hill JA, Zerr DM.** 2014. Roseoloviruses in transplant recipients: clinical consequences and prospects for treatment and prevention trials. Curr Opin Virol **9:**53-60.
5. **Arbuckle JH, Medveczky MM, Luka J, Hadley SH, Luegmayr A, Ablashi D, Lund TC, Tolar J, De Meirleir K, Montoya JG, Komaroff AL, Ambros PF, Medveczky PG.** 2010. The latent human herpesvirus-6A genome specifically integrates in telomeres of human chromosomes in vivo and in vitro. Proc Natl Acad Sci U S A **107:**5563-5568.
6. **Luppi M, Marasca R, Barozzi P, Ferrari S, Ceccherini-Nelli L, Batoni G, Merelli E, Torelli G.** 1993. Three cases of human herpesvirus-6 latent infection: integration of viral genome in peripheral blood mononuclear cell DNA. J Med Virol **40:**44-52.
7. **Luppi M, Barozzi P, Marasca R, Torelli G.** 1994. Integration of human herpesvirus-6 (HHV-6) genome in chromosome 17 in two lymphoma patients. Leukemia **8 Suppl 1:**S41-45.
8. **Daibata M, Taguchi T, Nemoto Y, Taguchi H, Miyoshi I.** 1999. Inheritance of chromosomally integrated human herpesvirus 6 DNA. Blood **94:**1545-1549.
9. **Tanaka-Taya K, Sashihara J, Kurahashi H, Amo K, Miyagawa H, Kondo K, Okada S, Yamanishi K.** 2004. Human herpesvirus 6 (HHV-6) is transmitted from parent to child in an integrated form and characterization of cases with chromosomally integrated HHV-6 DNA. J Med Virol **73:**465-473.
10. **Morissette G, Flamand L.** 2010. Herpesviruses and chromosomal integration. J Virol **84:**12100-12109.
11. **Pellett PE, Ablashi DV, Ambros PF, Agut H, Caserta MT, Descamps V, Flamand L, Gautheret-Dejean A, Hall CB, Kamble RT, Kuehl U, Lassner D, Lautenschlager I, Loomis KS, Luppi M, Lusso P, Medveczky PG, Montoya JG, Mori Y, Ogata M, Pritchett JC, Rogez S, Seto E, Ward KN, Yoshikawa T, Razonable RR.** 2012. Chromosomally integrated human herpesvirus 6: questions and answers. Rev Med Virol **22:**144-155.
12. **Gravel A, Dubuc I, Morissette G, Sedlak RH, Jerome KR, Flamand L.** 2015. Inherited chromosomally integrated human herpesvirus 6 as a predisposing risk factor for the development of angina pectoris. Proc Natl Acad Sci U S A **112:**8058-8063.
13. **Torelli G, Barozzi P, Marasca R, Cocconcelli P, Merelli E, Ceccherini-Nelli L, Ferrari S, Luppi M.** 1995. Targeted integration of human herpesvirus 6 in the p arm of chromosome 17 of human peripheral blood mononuclear cells in vivo. J Med Virol **46:**178-188.
14. **Daibata M, Taguchi T, Taguchi H, Miyoshi I.** 1998. Integration of human herpesvirus 6 in a Burkitt's lymphoma cell line. Br J Haematol **102:**1307-1313.
15. **Nacheva EP, Ward KN, Brazma D, Virgili A, Howard J, Leong HN, Clark DA.** 2008. Human herpesvirus 6 integrates within telomeric regions as evidenced by five different chromosomal sites. J Med Virol **80:**1952-1958.
16. **Takubo K, Aida J, Izumiyama-Shimomura N, Ishikawa N, Sawabe M, Kurabayashi R, Shiraishi H, Arai T, Nakamura K.** 2010. Changes of telomere length with aging. Geriatr Gerontol Int **10 Suppl 1:**S197-206.
17. **Makarov VL, Hirose Y, Langmore JP.** 1997. Long G tails at both ends of human chromosomes suggest a C strand degradation mechanism for telomere shortening. Cell **88:**657-666.
18. **McElligott R, Wellinger RJ.** 1997. The terminal DNA structure of mammalian chromosomes. EMBO J **16:**3705-3714.

19. **Chai W, Shay JW, Wright WE.** 2005. Human telomeres maintain their overhang length at senescence. Mol Cell Biol **25:**2158-2168.
20. **Zhang J, Rane G, Dai X, Shanmugam MK, Arfuso F, Samy RP, Lai MK, Kappei D, Kumar AP, Sethi G.** 2016. Ageing and the telomere connection: An intimate relationship with inflammation. Ageing Res Rev **25:**55-69.
21. **de Lange T.** 2009. How telomeres solve the end-protection problem. Science **326:**948-952.
22. **Gompels UA, Nicholas J, Lawrence G, Jones M, Thomson BJ, Martin ME, Efstathiou S, Craxton M, Macaulay HA.** 1995. The DNA sequence of human herpesvirus-6: structure, coding content, and genome evolution. Virology **209:**29-51.
23. **Dominguez G, Dambaugh TR, Stamey FR, Dewhurst S, Inoue N, Pellett PE.** 1999. Human herpesvirus 6B genome sequence: coding content and comparison with human herpesvirus 6A. J Virol **73:**8040-8052.
24. **Isegawa Y, Mukai T, Nakano K, Kagawa M, Chen J, Mori Y, Sunagawa T, Kawanishi K, Sashihara J, Hata A, Zou P, Kosuge H, Yamanishi K.** 1999. Comparison of the complete DNA sequences of human herpesvirus 6 variants A and B. J Virol **73:**8053-8063.
25. **Deng H, Dewhurst S.** 1998. Functional identification and analysis of cis-acting sequences which mediate genome cleavage and packaging in human herpesvirus 6. J Virol **72:**320-329.
26. **Thomson BJ, Dewhurst S, Gray D.** 1994. Structure and heterogeneity of the a sequences of human herpesvirus 6 strain variants U1102 and Z29 and identification of human telomeric repeat sequences at the genomic termini. J Virol **68:**3007-3014.
27. **Morissette G, Flamand L.** 2010. Herpesviruses and chromosomal integration, p 12100-12109, J Virol, vol 84, United States.
28. **Kaufer BB, Flamand L.** 2014. Chromosomally integrated HHV-6: impact on virus, cell and organismal biology. Curr Opin Virol **9C:**111-118.
29. **Wallaschek N, Sanyal A, Pirzer F, Gravel A, Mori Y, Flamand L, Kaufer BB.** 2016. The Telomeric Repeats of Human Herpesvirus 6A (HHV-6A) Are Required for Efficient Virus Integration. PLoS Pathog **12:**e1005666.
30. **Arbuckle JH, Pantry SN, Medveczky MM, Prichett J, Loomis KS, Ablashi D, Medveczky PG.** 2013. Mapping the telomere integrated genome of human herpesvirus 6A and 6B. Virology **442:**3-11.
31. **Huang Y, Hidalgo-Bravo A, Zhang E, Cotton VE, Mendez-Bermudez A, Wig G, Medina-Calzada Z, Neumann R, Jeffreys AJ, Winney B, Wilson JF, Clark DA, Dyer MJ, Royle NJ.** 2014. Human telomeres that carry an integrated copy of human herpesvirus 6 are often short and unstable, facilitating release of the viral genome from the chromosome, p 315-327, Nucleic Acids Res, vol 42, England.
32. **Ohye T, Inagaki H, Ihira M, Higashimoto Y, Kato K, Oikawa J, Yagasaki H, Niizuma T, Takahashi Y, Kojima S, Yoshikawa T, Kurahashi H.** 2014. Dual roles for the telomeric repeats in chromosomally integrated human herpesvirus-6. Sci Rep **4:**4559.
33. **Lipps HJ, Rhodes D.** 2009. G-quadruplex structures: in vivo evidence and function. Trends Cell Biol **19:**414-422.
34. **Sen D, Gilbert W.** 1990. A sodium-potassium switch in the formation of four-stranded G4-DNA. Nature **344:**410-414.
35. **Karsisiotis AI, Hessari NM, Novellino E, Spada GP, Randazzo A, Webba da Silva M.** 2011. Topological characterization of nucleic acid G-quadruplexes by UV absorption and circular dichroism. Angew Chem Int Ed Engl **50:**10645-10648.
36. **Read M, Harrison RJ, Romagnoli B, Tanious FA, Gowan SH, Reszka AP, Wilson WD, Kelland LR, Neidle S.** 2001. Structure-based design of selective and potent G quadruplex-mediated telomerase inhibitors. Proc Natl Acad Sci U S A **98:**4844-4849.
37. **Campbell NH, Parkinson GN, Reszka AP, Neidle S.** 2008. Structural basis of DNA quadruplex recognition by an acridine drug. J Am Chem Soc **130:**6722-6724.

38. **Zhou G, Liu X, Li Y, Xu S, Ma C, Wu X, Cheng Y, Yu Z, Zhao G, Chen Y.** 2016. Telomere targeting with a novel G-quadruplex-interactive ligand BRACO-19 induces T-loop disassembly and telomerase displacement in human glioblastoma cells. Oncotarget **7:**14925-14939.
39. **Siddiqui-Jain A, Grand CL, Bearss DJ, Hurley LH.** 2002. Direct evidence for a G-quadruplex in a promoter region and its targeting with a small molecule to repress c-MYC transcription. Proc Natl Acad Sci U S A **99:**11593-11598.
40. **Oganesian L, Bryan TM.** 2007. Physiological relevance of telomeric G-quadruplex formation: a potential drug target. Bioessays **29:**155-165.
41. **Simonsson T, Pecinka P, Kubista M.** 1998. DNA tetraplex formation in the control region of c-myc. Nucleic Acids Res **26:**1167-1172.
42. **Biffi G, Tannahill D, McCafferty J, Balasubramanian S.** 2013. Quantitative visualization of DNA G-quadruplex structures in human cells. Nat Chem **5:**182-186.
43. **Henderson A, Wu Y, Huang YC, Chavez EA, Platt J, Johnson FB, Brosh RM, Jr., Sen D, Lansdorp PM.** 2014. Detection of G-quadruplex DNA in mammalian cells. Nucleic Acids Res **42:**860-869.
44. **Haider SM, Neidle S, Parkinson GN.** 2011. A structural analysis of G-quadruplex/ligand interactions. Biochimie **93:**1239-1251.
45. **Gravel A, Dubuc I, wallaschek N, Gilbert-Girard S, Collin V, Hall-Sedlak R, Jerome KR, Mori Y, Carbonneau J, Boivin G, Kaufer BB, Flamand L.** 2017. Cell culture systems to study Human Herpesvirus 6A/B Chromosomal Integration. Journal of Virology **(In press)**.
46. **Osterrieder N, Wallaschek N, Kaufer BB.** 2014. Herpesvirus Genome Integration into Telomeric Repeats of Host Cell Chromosomes. Annual Review of Virology **1:**215-235.
47. **Endo A, Watanabe K, Ohye T, Suzuki K, Matsubara T, Shimizu N, Kurahashi H, Yoshikawa T, Katano H, Inoue N, Imai K, Takagi M, Morio T, Mizutani S.** 2014. Molecular and Virological Evidence of Viral Activation From Chromosomally Integrated Human Herpesvirus 6A in a Patient With X-Linked Severe Combined Immunodeficiency. Clin Infect Dis **59:**545-548.
48. **Gravel A, Hall CB, Flamand L.** 2013. Sequence analysis of transplacentally acquired human herpesvirus 6 DNA is consistent with transmission of a chromosomally integrated reactivated virus. J Infect Dis **207:**1585-1589.
49. **Hill JA, Sedlak RH, Zerr DM, Huang ML, Yeung C, Myerson D, Jerome KR, Boeckh MJ.** 2015. Prevalence of chromosomally integrated human herpesvirus 6 in patients with human herpesvirus 6-central nervous system dysfunction. Biol Blood Marrow Transplant **21:**371-373.
50. **Prusty BK, Krohne G, Rudel T.** 2013. Reactivation of chromosomally integrated human herpesvirus-6 by telomeric circle formation. PLoS Genet **9:**e1004033.
51. **Trempe F, Gravel A, Dubuc I, Wallaschek N, Collin V, Gilbert-Girard S, Morissette G, Kaufer BB, Flamand L.** 2015. Characterization of human herpesvirus 6A/B U94 as ATPase, helicase, exonuclease and DNA-binding proteins. Nucleic Acids Res **43:**6084-6098.
52. **Wallaschek N, Gravel A, Flamand L, Kaufer BB.** 2016. The putative U94 integrase is dispensable for human herpesvirus 6 (HHV-6) chromosomal integration. J Gen Virol doi:10.1099/jgv.0.000502.
53. **Branzei D, Foiani M.** 2008. Regulation of DNA repair throughout the cell cycle. Nat Rev Mol Cell Biol **9:**297-308.
54. **Cesare AJ, Reddel RR.** 2010. Alternative lengthening of telomeres: models, mechanisms and implications. Nat Rev Genet **11:**319-330.
55. **de Lange T.** 2005. Shelterin: the protein complex that shapes and safeguards human telomeres. Genes Dev **19:**2100-2110.
56. **Wang RC, Smogorzewska A, de Lange T.** 2004. Homologous recombination generates T-loop-sized deletions at human telomeres. Cell **119:**355-368.
57. **Min J, Wright WE, Shay JW.** 2017. Alternative lengthening of telomeres can be maintained by preferential elongation of lagging strands. Nucleic Acids Res doi:10.1093/nar/gkw1295.
58. **Chai W, Du Q, Shay JW, Wright WE.** 2006. Human telomeres have different overhang sizes at leading versus lagging strands. Mol Cell **21:**427-435.

59. **Wu G, Lee WH, Chen PL.** 2000. NBS1 and TRF1 colocalize at promyelocytic leukemia bodies during late S/G2 phases in immortalized telomerase-negative cells. Implication of NBS1 in alternative lengthening of telomeres. J Biol Chem **275:**30618-30622.
60. **Yeager TR, Neumann AA, Englezou A, Huschtscha LI, Noble JR, Reddel RR.** 1999. Telomerase-negative immortalized human cells contain a novel type of promyelocytic leukemia (PML) body. Cancer Res **59:**4175-4179.
61. **Opresko PL, Otterlei M, Graakjaer J, Bruheim P, Dawut L, Kolvraa S, May A, Seidman MM, Bohr VA.** 2004. The Werner syndrome helicase and exonuclease cooperate to resolve telomeric D loops in a manner regulated by TRF1 and TRF2. Molecular cell **14:**763-774.
62. **Schawalder J, Paric E, Neff NF.** 2003. Telomere and ribosomal DNA repeats are chromosomal targets of the bloom syndrome DNA helicase. BMC Cell Biol **4:**15.
63. **Stavropoulos DJ, Bradshaw PS, Li X, Pasic I, Truong K, Ikura M, Ungrin M, Meyn MS.** 2002. The Bloom syndrome helicase BLM interacts with TRF2 in ALT cells and promotes telomeric DNA synthesis. Hum Mol Genet **11:**3135-3144.
64. **Chatterjee S, Zagelbaum J, Savitsky P, Sturzenegger A, Huttner D, Janscak P, Hickson ID, Gileadi O, Rothenberg E.** 2014. Mechanistic insight into the interaction of BLM helicase with intra-strand G-quadruplex structures. Nat Commun **5:**5556.
65. **Fry M, Loeb LA.** 1999. Human werner syndrome DNA helicase unwinds tetrahelical structures of the fragile X syndrome repeat sequence d(CGG)n. J Biol Chem **274:**12797-12802.
66. **Sun H, Karow JK, Hickson ID, Maizels N.** 1998. The Bloom's syndrome helicase unwinds G4 DNA. J Biol Chem **273:**27587-27592.
67. **Li JL, Harrison RJ, Reszka AP, Brosh RM, Jr., Bohr VA, Neidle S, Hickson ID.** 2001. Inhibition of the Bloom's and Werner's syndrome helicases by G-quadruplex interacting ligands. Biochemistry **40:**15194-15202.
68. **Metifiot M, Amrane S, Litvak S, Andreola ML.** 2014. G-quadruplexes in viruses: function and potential therapeutic applications. Nucleic Acids Res **42:**12352-12366.
69. **Artusi S, Nadai M, Perrone R, Biasolo MA, Palu G, Flamand L, Calistri A, Richter SN.** 2015. The Herpes Simplex Virus-1 genome contains multiple clusters of repeated G-quadruplex: Implications for the antiviral activity of a G-quadruplex ligand. Antiviral Res **118:**123-131.
70. **Norseen J, Johnson FB, Lieberman PM.** 2009. Role for G-quadruplex RNA binding by Epstein-Barr virus nuclear antigen 1 in DNA replication and metaphase chromosome attachment. J Virol **83:**10336-10346.
71. **Biswas B, Kandpal M, Jauhari UK, Vivekanandan P.** 2016. Genome-wide analysis of G-quadruplexes in herpesvirus genomes. BMC Genomics **17:**949.
72. **Bodnar AG, Ouellette M, Frolkis M, Holt SE, Chiu CP, Morin GB, Harley CB, Shay JW, Lichtsteiner S, Wright WE.** 1998. Extension of life-span by introduction of telomerase into normal human cells. Science **279:**349-352.
73. **Harley CB, Futcher AB, Greider CW.** 1990. Telomeres shorten during ageing of human fibroblasts. Nature **345:**458-460.
74. **Hemann MT, Strong MA, Hao LY, Greider CW.** 2001. The shortest telomere, not average telomere length, is critical for cell viability and chromosome stability. Cell **107:**67-77.
75. **Capper R, Britt-Compton B, Tankimanova M, Rowson J, Letsolo B, Man S, Haughton M, Baird DM.** 2007. The nature of telomere fusion and a definition of the critical telomere length in human cells. Genes & development **21:**2495-2508.
76. **Gravel A, Ablashi D, Flamand L.** 2013. Complete Genome Sequence of Early Passaged Human Herpesvirus 6A (GS Strain) Isolated from North America. Genome Announc **1**.
77. **Huffman KE, Levene SD, Tesmer VM, Shay JW, Wright WE.** 2000. Telomere shortening is proportional to the size of the G-rich telomeric 3'-overhang. J Biol Chem **275:**19719-19722.
78. **Lusso P, Markham PD, Tschachler E, di Marzo Veronese F, Salahuddin SZ, Ablashi DV, Pahwa S, Krohn K, Gallo RC.** 1988. In vitro cellular tropism of human B-lymphotropic virus (human herpesvirus-6). The Journal of experimental medicine **167:**1659-1670.

79. **Hiyama K, Hirai Y, Kyoizumi S, Akiyama M, Hiyama E, Piatyszek MA, Shay JW, Ishioka S, Yamakido M.** 1995. Activation of telomerase in human lymphocytes and hematopoietic progenitor cells. J Immunol **155:**3711-3715.

80. **Weng NP, Levine BL, June CH, Hodes RJ.** 1996. Regulated expression of telomerase activity in human T lymphocyte development and activation. J Exp Med **183:**2471-2479.

81. **Flamand L, Gosselin J, D'Addario M, Hiscott J, Ablashi DV, Gallo RC, Menezes J.** 1991. Human herpesvirus 6 induces interleukin-1 beta and tumor necrosis factor alpha, but not interleukin-6, in peripheral blood mononuclear cell cultures. J Virol **65:**5105-5110.

82. **Jaworska J, Gravel A, Fink K, Grandvaux N, Flamand L.** 2007. Inhibition of transcription of the beta interferon gene by the human herpesvirus 6 immediate-early 1 protein. J Virol **81:**5737-5748.

83. **Sedlak RH, Cook L, Huang ML, Magaret A, Zerr DM, Boeckh M, Jerome KR.** 2014. Identification of chromosomally integrated human herpesvirus 6 by droplet digital PCR. Clin Chem **60:**765-772.

84. **Flamand L, Gravel A, Boutolleau D, Alvarez-Lafuente R, Jacobson S, Malnati MS, Kohn D, Tang YW, Yoshikawa T, Ablashi D.** 2008. Multicenter comparison of PCR assays for detection of human herpesvirus 6 DNA in serum. J Clin Microbiol **46:**2700-2706.

638 Legend to figure 1: Specificity of the BG4 and 1H6 antibodies for G-quadruplex structures. Binding
639 curves as determined by ELISA showing that the BG4 (A) and 1H6 (B) antibodies have high affinity for
640 intramolecular DNA G-quadruplex structures (myc and Telo-(TTAGGG)) relative to non G-quadruplex
641 containing DNA (ss-DNA). Results (absorbance at 450 nm) are expressed as mean± SD of 4
642 independent experiments.

643

644 Legend to figure 2: Association and dissociation curves of ligands (BG4 and BRACO-19) to the DNA
645 oligos by surface plasmon resonance. Curves of the association and dissociation over time between
646 the ligands (BG4 antibody and BRACO-19) and the DNA sequences (myc promoter, Telo G-rich
647 telomere $(TTAGGG)_4$ and C-rich telomere $(CCCTAA)_4$), corresponding to association (Ka), dissociation
648 (Kd) and equilibrium (KD) constants. Curves with BG4 (0 nM - 800 nM) are from A to C and curves with
649 BRACO-19 (0 nM - 100 nM) are from D to F.

650

651 Legend to figure 3. CD spectra and thermal unfolding ofHHV-6A *pac1* and telomeric (Telo)
652 $AGGG(TTAGGG)_3$ oligonucleotides. A-B) CD spectra and thermal unfolding of HHV-6A *pac1*
653 oligonucleotide in the absence (A) or in the presence of 100 mM K^+ (B). C) CD spectra and thermal
654 unfolding of telomeric oligonucleotides in the presence of 100 mM K^+. D) CD spectra of telomeric
655 oligonucleotide in the absence of in the presence of BRACO-19 (16µM). E) CD spectra and thermal
656 unfolding of telomeric oligonucleotide in the presence of 100 mM KCl and BRACO-19 (16µM). F)
657 Relative melting curves of the telomeric oligonucleotides in the absence or in the presence of BRACO-
658 19 (16 µM) plotted at the wavelength corresponding to the maximum of CD signal (291 nm).

659

Legend to figure 4. Determination of BRACO-19 toxicity. U2OS, HeLa and MCF-7 cells were incubated with indicated concentrations of BRACO-19 for 3 days, after which cell number and viability were determined using the MTT assay. Results are expressed as mean ratio ± SD relative to control in the absence of BRACO-19. *p<0.05.

Legend to figure 5. Effects of BRACO-19 on intracellular HHV-6 DNA levels. A) U2OS, HeLa and MCF-7 cells were infected with HHV-6A and incubated with 1 µM BRACO-19 for 4h, 48h and 72h after which the intracellular HHV-6 DNA content was estimated by qPCR. Results are expressed as mean ± SD (n=4) HHV-6 DNA levels relative to cellular DNA (GAPDH gene) following normalization to the 4h BRACO-19 untreated time point. *p<0.05. B) U2OS cells were infected with HHV-6A and 48h later the cells were processed for IFA using anti-immediate-early 1 antibodies or anti-P41 (early) antibodies. C) Metaphase spread of a HeLa ciHHV-6A+ clone. The HHV-6A genome was detected using a DIG-labeled probe (green) by FISH. Chromosomes are visualized using DAPI (blue).

Figure 1

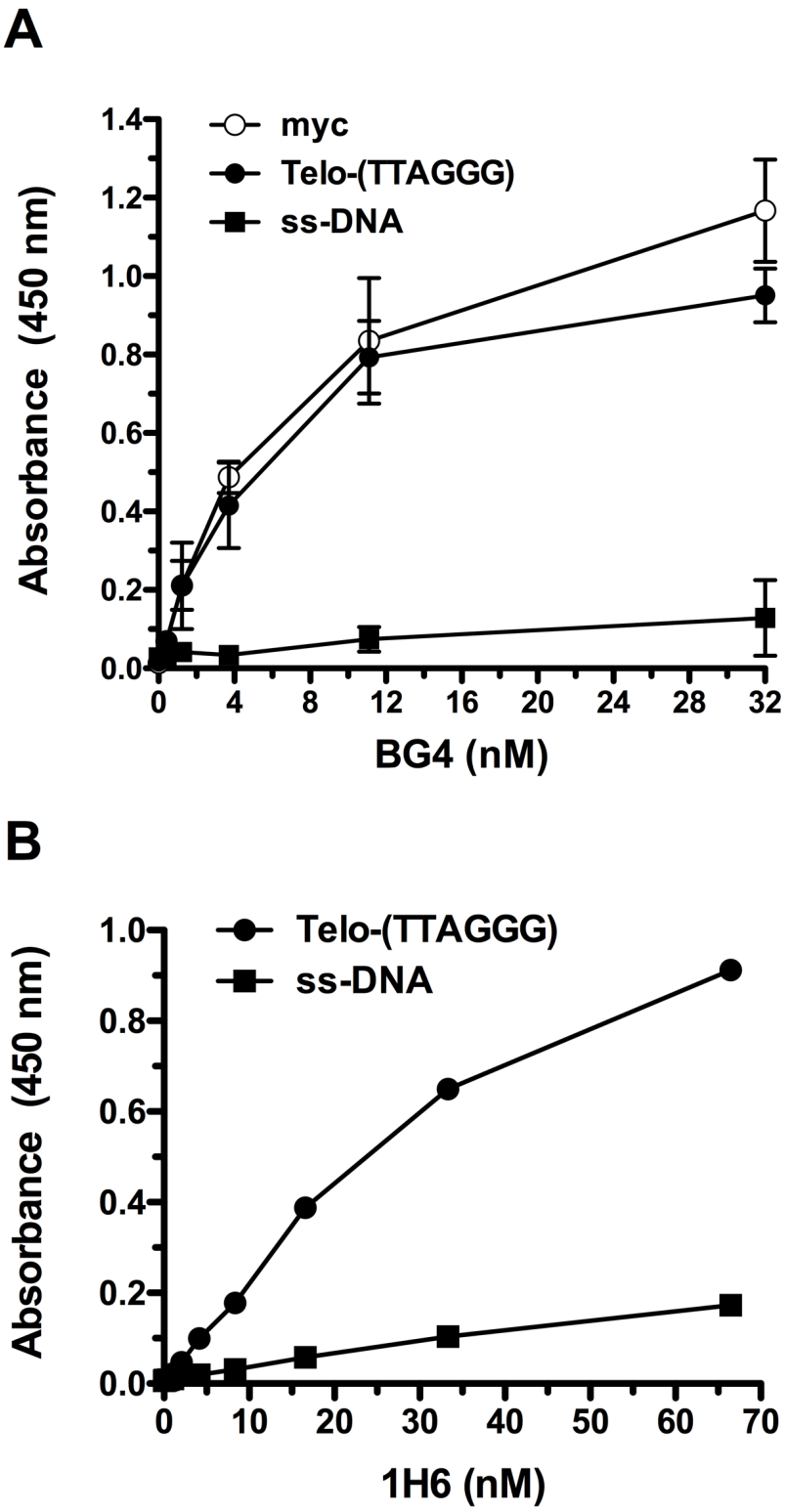

Figure 2

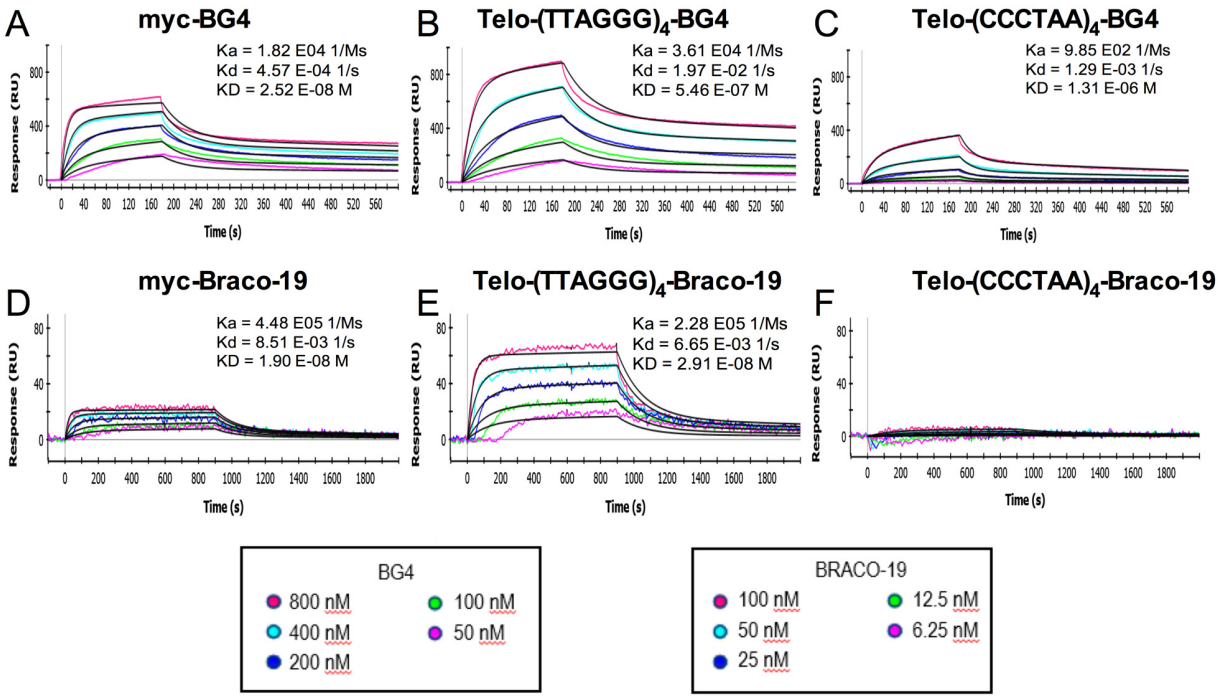

Figure 3

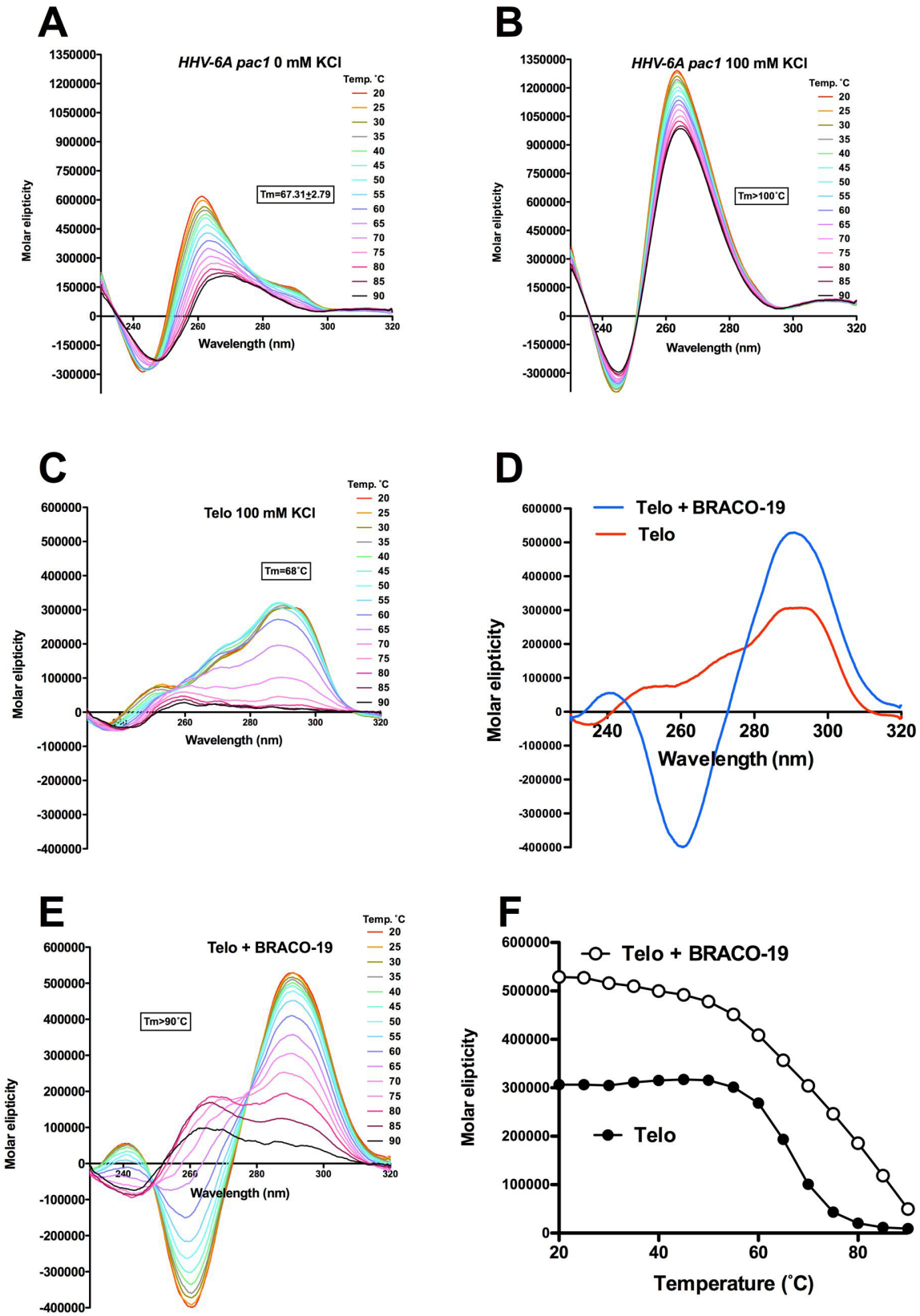

Figure 4

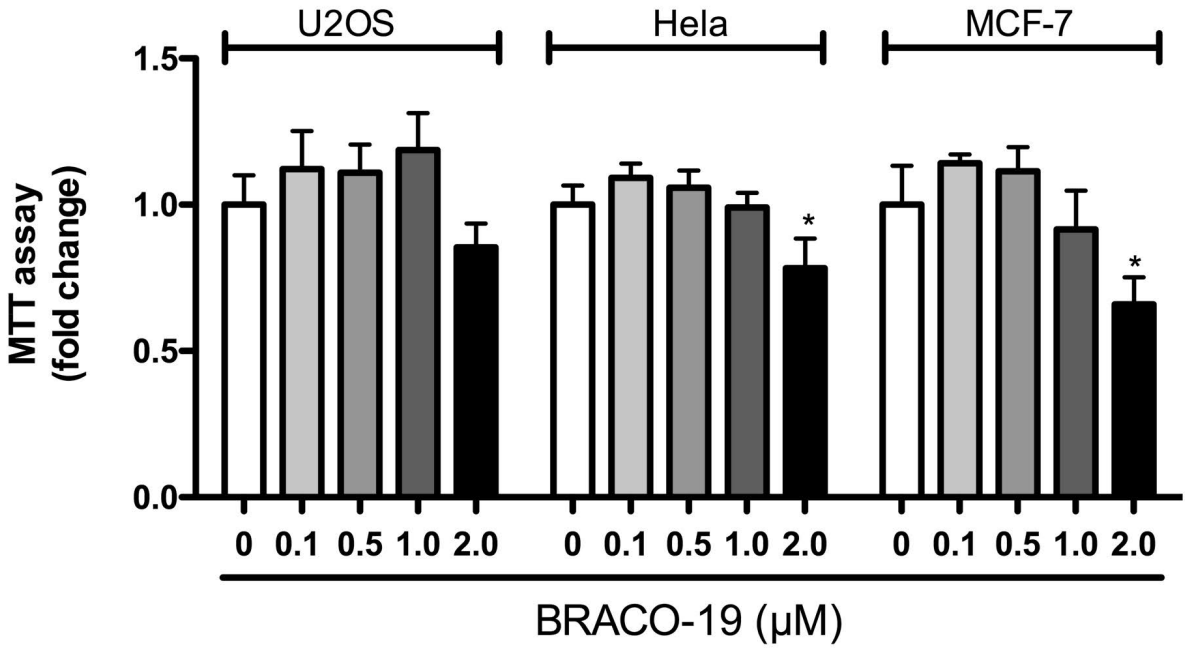

Figure 5

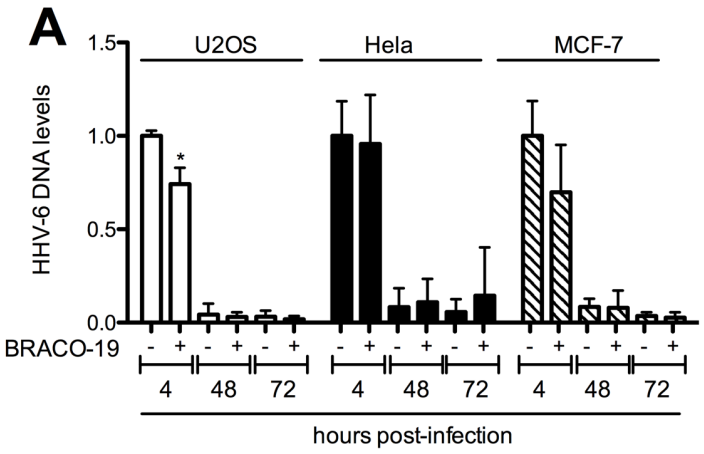

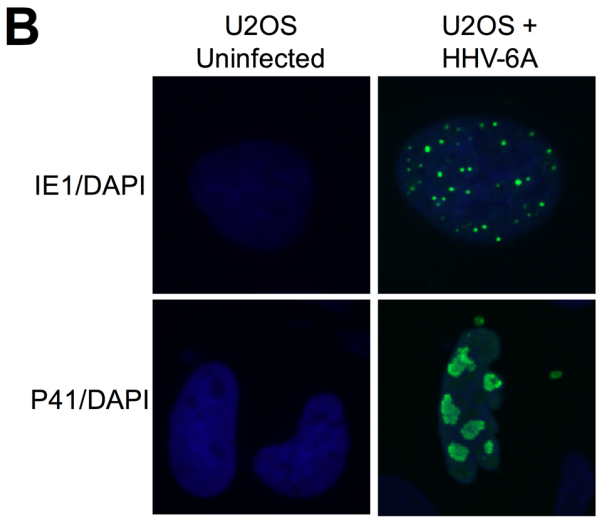

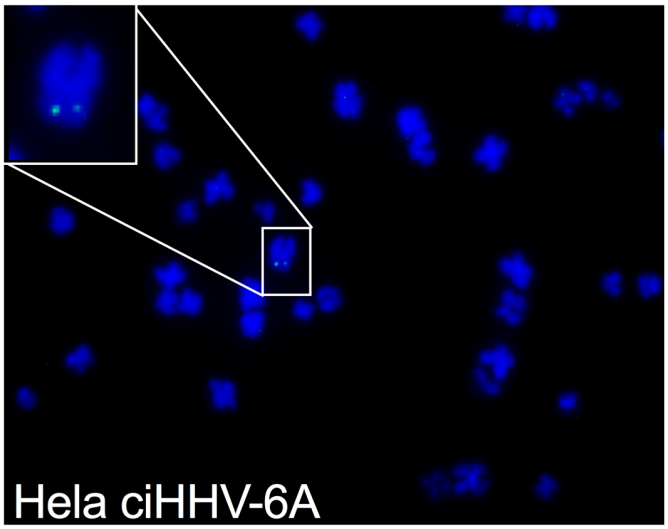

Table 1. Effects of BRACO-19 on HHV-6A integration frequency in HeLa and U2OS cells.

HeLa	*ciHHV-6 - clones*	*ciHHV-6+ clones*	*Integration frequency*
HeLa	413	82	16.6%
HeLa +BRACO-19	338	34	9.1%*
U2OS	202	17	7.8%
U2OS +BRACO-19	137	11	7.4%

* p=0.0017

Table 2. Effects of BRACO-19 on chromosomal integration of HHV-6A into HeLa, MCF-7 and U2OS cells.

	N copies of U65-U66/ *N* copies of RPP30	% of ciHHV-6A+ cells
HeLa	42.2/1070	7,9
HeLa +BRACO-19	16.7/893	3,74*
MCF-7	40.1/701	11,4
MCF-7 +BRACO-19	18.6/665	5,58**
U2OS	151/1683	18
U2OS +BRACO-19	67.6/980	13,8

*p =0.010 **p=0.009